Polymer 51 (2010) 554–562

Contents lists available at ScienceDirect

Polymer

journal homepage: www.elsevier.com/locate/polymer

Labyrinthine pattern of polymer crystals from supercooled ultrathin films

Guoliang Zhang [a], Liuxin Jin [a], Ping Zheng [a], An-Chang Shi [b], Wei Wang [a,*]

[a] The Key Laboratory of Functional Polymer Materials of Ministry of Education and Institute of Polymer Chemistry, College of Chemistry, Nankai University, Tianjin 300071, P.R. China
[b] Department of Physics and Astronomy, McMaster University, Hamilton, Ontario L8S 4M1, Canada

ARTICLE INFO

Article history:
Received 15 September 2009
Received in revised form
19 November 2009
Accepted 29 November 2009
Available online 4 December 2009

Keywords:
Crystal pattern
Labyrinth
Ultrathin film

ABSTRACT

We report the observation of a labyrinthine crystal pattern with a periodic structure in the crystal width direction in ultrathin films of poly(ethylene oxide) fractions with molecular weight ranging from 25,000 to 932,000 g/mol. The polymer thin films are crystallized at temperatures well below the bulk melting temperature, thus the system is characterized by limited diffusion of the polymer chains and rapid growth of the crystal fronts. The competition of these two competing factors leads to the formation of the labyrinthine pattern. This mechanism is supported by a scaling relation between the long period and molecular weight, $\bar{L} \propto \bar{M}_w^{-0.24\pm0.03}$, indicating the importance of chain diffusion. Furthermore, a linear relationship between $\ln(\bar{L}/\bar{M}_w^{-0.24})$–$\Delta E/RT_c$ and $T_m^0/T_c\Delta T$ is observed, implying that the crystal growth is dominated by a secondary nucleation.

1. Introduction

The formation of various intricate patterns in nature have attracted tremendous attention in the past decades [1]. Normally, the formation of complex patterns under nonequilibrium conditions is due to the growth instability in a diffusion field [2–4]. Crystal patterns such as dendrite, seaweed, and compact structures have been extensively studied [5–11]. Recently, transitions among the different patterns of crystalline polymers have been investigated [12–15]. It is widely accepted that the combination of the diffusion-limited-aggregation (DLA) model [16], which is a typical nonlocal growth model [17], with the surface kinetic process [13,14] can provide a basic description of the underlying physics of these complex patterns in the regime where diffusion is sufficiently fast. It has been also noticed that the DLA process is not in operation when the crystallization rate is faster than the molecular diffusion rate in a local-diffusion field far from equilibrium [18–20]. In the regime where the diffusion is very slow and the crystal growth is fast, it is not clear what type of crystal patterns will form and what the pattern formation mechanism is in operation. Besides significance in polymer physics, solving this problem can also shed light to the understanding of the liquid/melt-to-solid phase transition behaviors in local-diffusion field in condensed matter physics [21,22]. Currently, it is well recognized that two requirements must be satisfied to realize a local-diffusion field for the study of pattern formation in this regime: (1) a slow diffusion of the molten materials and (2) a rapid growth of the crystal fronts. Based on our previous studies on crystal patterns of crystalline polymers [13,14,23] we believe that polymer crystallization from ultrathin films can satisfy these two requirements. First of all, due to the elevated glass transition temperature (T_g) and the deformed pancake-like conformation of the adsorbed chains, the polymers in ultrathin polymer films on solid substrates execute confined motion in quasi-2-diemnsional space (quasi-2D).[24–27] Therefore, the first requirement of slow diffusion can be satisfied, especially at low temperatures. To satisfy the second requirement of fast growth, we can simply set the crystallization temperatures (T_cs) near the maximal-crystallization-rate-temperature.

Because of their long chain nature, polymer crystallization is one of the most mysterious topics in polymer science [28–30]. It is generally observed that polymer chains prefer to fold several times, forming folded-chain lamellar crystals whose thickness is normally less than the contour length of macromolecules. Nucleation theory proposed by Hoffman and Lauritzen [31] (HL) and precursor theory recently proposed by Strobl [32] are two important models which have been widely used to describe the polymer crystallization processes. In the HL theory, second nucleation and lateral growth are used to describe the growth of polymer lamellar crystals. A polymer chain firstly nucleates on crystal growing front, and then joins the crystal via lateral growth. According to the relationships between second nucleation rate and lateral growth rate at different supercoolings, polymer crystallization could be divided into three regimes. Because the trajectory of an individual polymer chain is difficult to be specified, the analyses of polymer crystallization are

* Corresponding author. Fax: +86 22 2349 8126.
E-mail address: weiwang@nankai.edu.cn (W. Wang).

0032-3861/$ – see front matter © 2009 Elsevier Ltd. All rights reserved.
doi:10.1016/j.polymer.2009.11.061

based on the assumption of consistency between microscopic and macroscopic pictures. In the precursor theory, polymer chains are assumed to firstly form a mesomorphic layer which spontaneously thickens up to a critical value, then transform into a granular crystalline layer, and at last convert to homogeneous lamellar crystallites. Many experiments have elucidated the rationality of these theories. However, it is worth to mention that most polymers used in these experiments were fractions with low-molecular-weights (LMW). For instance, the molecular weights of most poly(ethylene oxide) (PEO) fractions used in previous studies were not higher than 20,000 g/mol.[11,33–55] Undoubtedly, studies on crystallization habits of high-molecular-weight (HMW) fractions are very important to gain insight into the effects of some complex but important features, such as chain entanglement and conformation, on polymer crystallization [27,56–59].

In this study, we will firstly demonstrate and characterize a novel labyrinthine pattern formed from supercooled ultrathin films of a series of HMW PEO fractions, with different molecular weights in a wide range from 25,000 to 932,000 g/mol. Then, a local-diffusion-limited growth mechanism, or a local mass transport to the growing front mechanism, will be evoked to understand the labyrinthine pattern formation. The scaling relation between the long period in the crystal width direction and molecular weight will be employed to further elucidate the formation mechanism of this special pattern. We will explore the secondary nucleation effect on the temperature dependence of long period. The crystallization habits of these PEO fractions will also be discussed when the gyration diameter of polymer chains in the ultrathin film is larger than the long period of the crystal pattern.

2. Experimental section

HMW PEO fractions were purchased from Polymer Source and Polymer Standards Service GmbH. Four important parameters of these polymers are listed in Table 1. The molecular weights of these PEO fractions are much higher than the bulk PEO's entanglement molecular weight of 6800 g/mol [60]. Therefore, molecular diffusion of these polymers will be highly confined. The relatively narrow molecular weight distributions minimize the effect of polydispersity on the pattern features. The particular PEO samples are hydroxyl-terminated at one end and methyl-terminated at the other end. Toluene solutions of these PEO fractions with a concentration of 0.01–0.02 wt.% were prepared in glassware. Silicon wafers with a size of about 0.8 × 0.8 cm^2 were treated in the Piranha solution of H_2SO_4 (98%):H_2O_2 (30%) = 3:1 at ~120 °C for 30 min to add a layer of −OH groups at the silicon surfaces and then cleaned in an ultrasonic water bath. The −OH layer may prevent the epitaxy growth of PEO on crystalline silicon surface. We measured the contact angle, A, of water on the surface of silicon wafer. The value of A is 8° for the surface of treated silicon wafers, while $A = 55°$ for the un-treated silicon wafers. Thus the treated surface was hydrophilic and the interaction between PEO and silicon surface was very strong, because PEO is also hydrophilic. Ultrathin PEO films were prepared by dropping the solution (3–4 μl) onto silicon surfaces at room temperature. The samples were dried at ambient condition overnight and then treated in vacuo at room temperature for 12 h. The as-prepared samples were firstly heated to 80.0 °C for 5 min to form a uniform molten layer and then were cooled to the specific T_cs to let the supercooled melt recrystallize for 5 h. A hot-stage multimode atomic force microscope (AFM, Digital Instrumental Nanoscope IV) operated in tapping mode was used to visualize crystal patterns.

Table 1
Molecular parameters of the PEO fractions.

Sample designation	$\overline{M}_w$, g/mol	$\overline{M}_w/\overline{M}_n$	T_m^0, °C	R_g, nm
25k-PEO	25,000	1.17	67.4	6.8
35k-PEO	35,000	1.23	67.8	8.1
116k-PEO	116,000	1.18	68.6	14.7
205k-PEO	205,000	1.18	68.8	19.5
932k-PEO	932,000	1.11	69.0	41.6

$\overline{M}_w$ is weight-average molecular weight of polymers. $\overline{M}_w/\overline{M}_n$ means the polydispersity index of molecular weight. T_m^0 is the equilibrium melting point. R_g is the gyration radius in bulk calculated according to ref. [47].

3. Results and discussion

3.1. Labyrinthine crystal patterns

The most interesting observation from our experiments is the labyrinthine crystal patterns formed at crystallization temperatures in the range from 20 to 34 °C (or supercooling range from 49 to 35 °C), as shown in Fig. 1. These crystallization temperatures are lower than those at which dendrites were observed for the same PEO fractions. Crystal patterns such as labyrinthine, dendrite, four-fold symmetric compact structure, and faceted crystal observed at different temperature ranges are shown in Fig. 2 for an individual PEO fraction. Therefore we can conclude that the labyrinthine crystal patterns form in conditions farther from equilibrium than the dendrites. These labyrinthine patterns are remarkably different from the isotropic random labyrinthine patterns found in other systems [61–66]. In our system, crystal branches take an anisotropic growth along preferential crystallographic directions normal to (120) or (100)/(010) plane for PEO [67,68]), so the stripe-like crystal (SC) branches are either parallel or perpendicular to their neighbors. The thickness, l_c, of labyrinthine crystals for different PEO fractions is shown in Fig. 3. In the crystallization temperature range, the value of l_c increases slightly in vicinity of 7.0 nm with increasing T_c. It is noticed that this thickness is much smaller than the contour length of the PEO fractions, implying that the PEO chains are folded several times to form the crystals.

It is significant to relate our observation to the application of LMW PEO fractions in micropattern and nanoimprint studies [69,70]. In the LMW PEO cases the crystals were randomly growing, not necessarily following the pre-prepared micropattern directions. Our results may provide a method to obtain more ordered micropatterns and nanoimprints because of the anisotropic crystal growth.

3.2. Characteristics of labyrinthine pattern

The characteristics of the labyrinthine pattern are very different from those of the dendrite pattern found in PEO samples under anisotropic-DLA conditions [13,14]. Firstly, the labyrinthine pattern possesses a periodic structure in crystal width directions due to the identical width of branches and identical distance between parallel neighbors. The periodic nature of these patterns has been analyzed using fast-Fourier-transition (FFT) as shown in Fig. 4. Fig. 4b is the 2D intensity pattern (512 × 512 pixels) of Fig. 4a obtained using FFT. Four strong scattering spots in Fig. 4b indicate the long period of SCs in width directions. (Note that this FFT pattern obtained from the 2D periodic crystal pattern is totally different from scattering patterns of bulk samples which reflect periodic lamellar structure in 3D space.) After integrating the azimuthal intensity of Fig. 4b, we can get a circularly averaged integral image as shown in Fig. 4c. The strongest intensity peak, Q_{peak}, in Fig. 4c corresponds to the strong scattering spots in Fig. 4b. Certainly, dendrite pattern does not have such a periodic feature. Secondly, it is hard to differentiate main branches from side branches in the labyrinthine pattern as shown

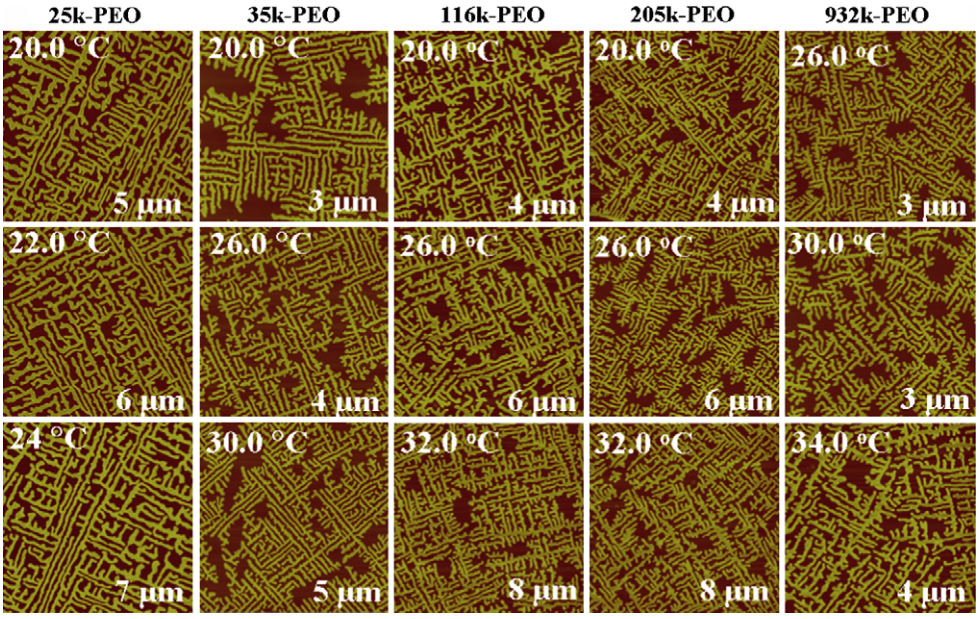

Fig. 1. AFM height images showing the labyrinthine crystal patterns of the different PEO fractions at different T_c s.

in Fig. 5a; while dendrite patterns normally show the distinct main and side branches, at least in size. Thirdly, different portions of the labyrinthine pattern may demonstrate unlike morphological features as shown in Fig. 5b; while every individual dendrite shows a similar tree-like feature, which corresponds to the "self-similarity" characteristic of DLA model. These characteristics certainly reflect that the formation mechanism of the labyrinthine pattern is different from that of dendrite.

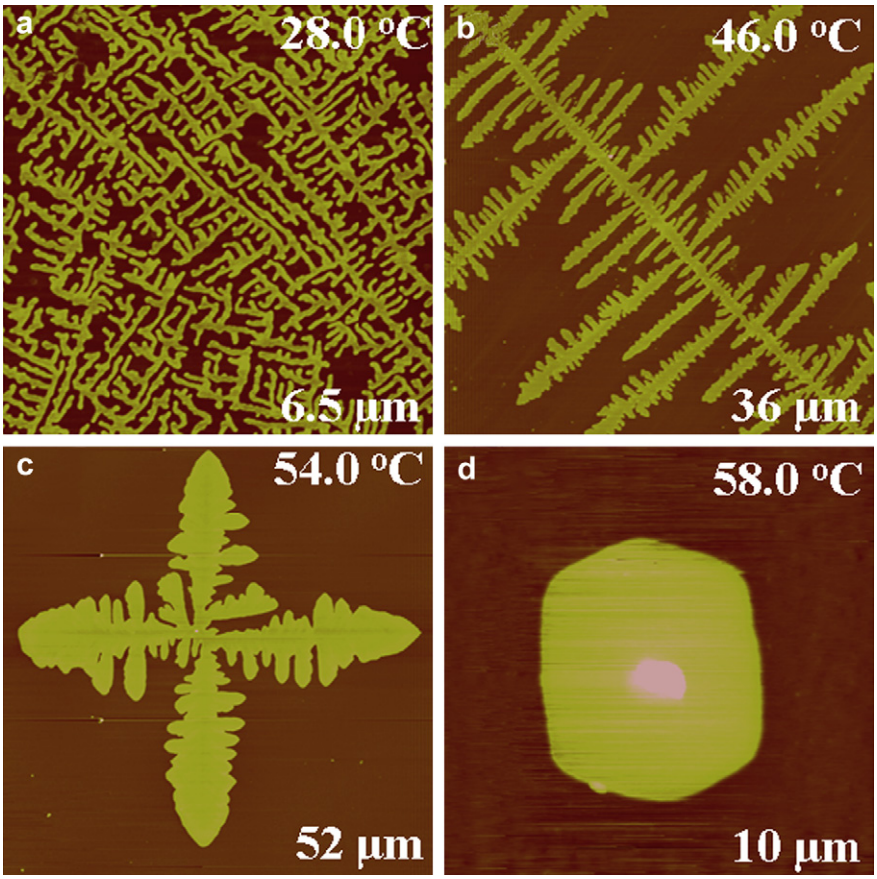

Fig. 2. Crystal patterns of (a) labyrinthine; (b) dendrite; (c) four-fold symmetric compact structure; (d) and faceted crystal observed at different temperatures for 116 k-PEO.

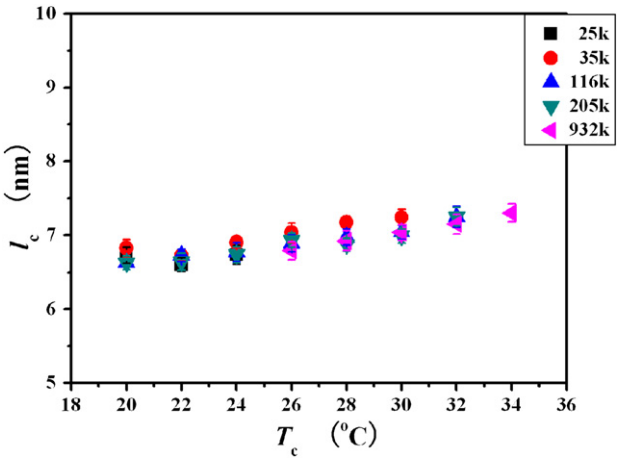

Fig. 3. Plot of l_c vs. T_c of different PEO fractions.

3.3. Local-diffusion field

The thickness of the ultrathin melt before recrystallization can be estimated from mass conservation, leading to the relation $l_a = \phi_c l_c \rho_c / \rho_a$, where l_a is the thickness of the ultrathin melt, ϕ_c is the coverage degree of crystals in silicon surfaces, $\rho_c = 1.234$ g/cm^{3}and $\rho_a = 1.124$ g/cm^3 are the densities of crystalline and molten PEO, respectively [71]. From the digital AFM images of typical labyrinthine crystal samples, it is found that $l_c \approx 7.0$ nm and $\phi_c \approx 50\%$. From these results, the value of l_a is estimated at about 4.0 nm, which is consistent with reported values [23,54,72]. The thickness of the ultrathin films is thinner than the crystal thickness, l_c, and much smaller than the gyration radius, R_g, of PEO fractions in bulk as shown in Table 1. From these results we can conclude that the PEO chains should have a pancake-like conformation caused by multiple, strong interactions between the silicon wafer surface and the PEO chains. The change of glass transition temperature of polymer thin films compare to that in bulk is highly dependent on the interaction between thin film and substrate surface. Weak interaction can decrease T_g and strong interaction can increase T_g [73–75]. The strong interaction between PEO and the hydrophilic silicon surface could raise T_g to 20 °C that is about 30 °C higher than that in bulk [27]. Meanwhile, the diffusion ability of macromolecules will be severely reduced with increasing molecular weight. Based on the empirical formula of maximal-crystallization-rate-temperature $T_{max} = 0.63T_m^0 + 0.37T_g - 18.5$, we obtain $T_{max} \approx 291.6\text{K} = 18.5$ °C for the PEO fractions. This temperature is in the vicinity of T_c range in our experiment. In the labyrinthine pattern formation process, unfortunately, the crystal growth is so fast that we cannot perform an in-situ observation using AFM to determine the growth rate (it needs about 5 min to capture an AFM image). From these physical quantities we can conclude that the crystal pattern formation conditions are under a slow molecular diffusion and a rapid crystal growth, that is, in a local-diffusion field.

3.4. Local-diffusion-limited growth mechanism

Because of the slow molecular diffusion and rapid crystal growth in the local-diffusion field, the supercooled molten macromolecules can only execute short diffusion steps in the growing front vicinity before joining crystals. In other words, the diffusion of the supercooled molten macromolecules is restricted in the area around the growing fronts. Thus the formation mechanism of the labyrinthine pattern follows a local-diffusion-limited

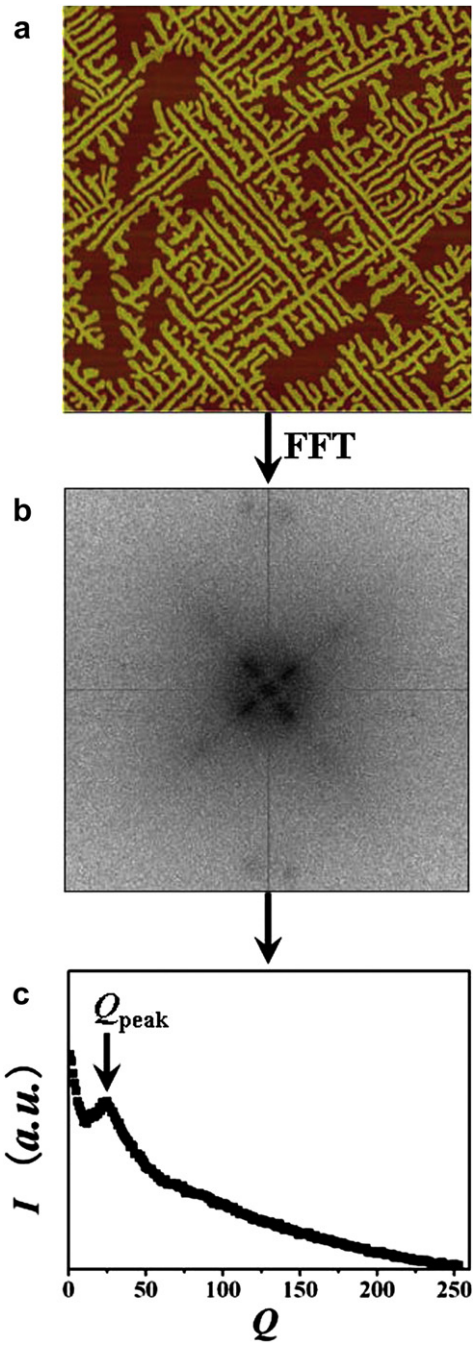

Fig. 4. (a) A typical labyrinthine pattern; (b) 2D FFT pattern of the labyrinthine pattern shows four scattering spots; (c) Circular average integral curve of the 2D FFT pattern.

process. Moreover, the local-diffusion field can only influence the growing front it surrounds. Generically, this mechanism provides a basic description for liquid/melt-to-solid phase transition in local-diffusion field. The relationship of $l_a < l_c$ implies that a depletion zone exists between the crystal growing front and the supercooled melt as shown in Fig. 6. $\overline{d}_c$ is the depletion zone length, which means a critical diffusion distance for supercooled molten macromolecules at a specified T_c before they join the growing fronts. If the distance between the ultrathin supercooled melt and growing front d is larger than $\overline{d}_c$, supercooled molten macromolecules cannot diffuse over the distance to join the growing front. When the distance between two parallel SCs d_{SC} is larger than $2\overline{d}_c$, some

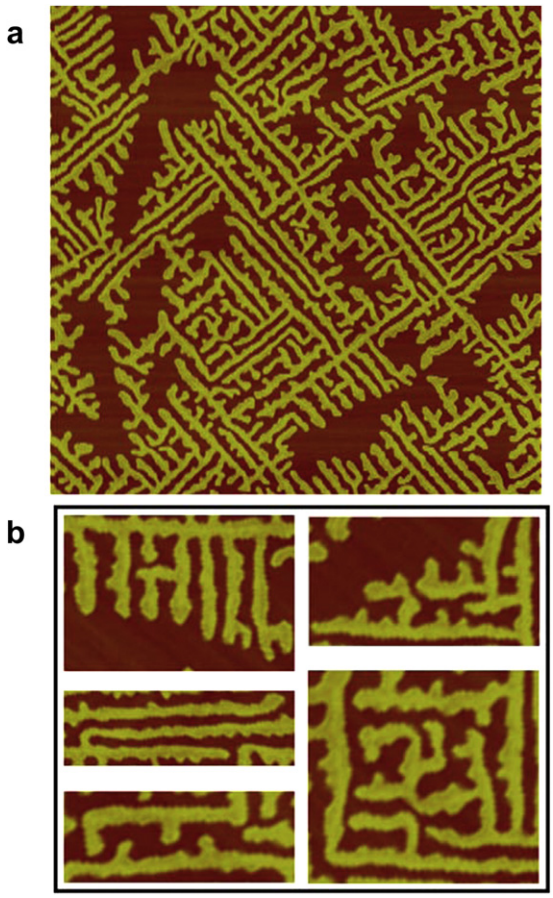

Fig. 5. (a) Typical labyrinthine crystal pattern of a PEO fraction with a molecular weight of 35,000 g/mol; (b) Five portions of the labyrinthine show unlike morphological features.

molten macromolecules may be left between the SCs. If $d_{sc} = 2\overline{d}_c$, there are no molten macromolecules left, then the average long period in the crystal width direction between parallel SCs is $\overline{L} = \overline{W} + 2\overline{d}_c$, where $\overline{W}$ is the average width of SCs.

3.5. Formation processes of different labyrinthine portions

Because of the local-diffusion nature of the supercooled molten macromolecules, the labyrinthine branch growths may be highly influenced by the local environments (such as the distribution of supercooled molten macromolecules, constraint of developing or developed crystals) surrounding the growing fronts. So, different portions of the labyrinthine pattern may demonstrate different morphological features. Some of them are highlighted in Fig. 5b. By analyzing the relations between d_{SC} and $\overline{d}_c$, we can reconstruct the rational formation processes of these different labyrinthine portions as shown in Fig. 7. The labyrinthine portion in Fig. 7a is composed of many parallel SCs where the distance between parallel neighbors is $d_{SC} \approx 2\overline{d}_c$. Firstly, an original stripe-like crystal formed as shown in Fig. 7a$_1$. Supercooled melt distributed near the original SC, and there were no other crystals. Then, many small parallel SCs propagated from the original SC and were growing almost at the same time as shown in Fig. 7a$_2$. When the supercooled melt nearby were exhausted, the parallel SCs stopped growing and an array-like portion formed. In Fig. 7b, the side-branched-SC formation should be due to discontinuous distribution of the supercooled melt between two parallel neighbors where

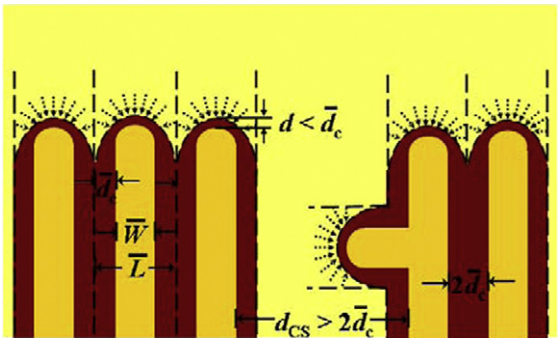

Fig. 6. Schematics of the growth of the labyrinthine crystal branches and the definition of the character lengths of $\overline{d}_c$, $\overline{W}$ and $\overline{L}$. d is the distance between the supercooled melt and growing front, and d_{SC} is the distance between two parallel SC neighbors. Deep yellow regions represent SCs. Light yellow regions represent ultrathin supercooled melt. Deep red regions represent depletion zones. (For interpretation of the references to colour in this figure legend, the reader is referred to the web version of this article.)

$2\overline{d}_c < d_{SC} < \overline{L} + 2\overline{d}_c$ as shown in Fig. 7b$_1$ and 6b$_2$. In the labyrinthine patterns, a stripe-like crystal may take a turn of 90° (SC-90°) as shown in Fig. 7c, d and e enclosed by white circles. The formation of the SC-90° was attributable to that the growing tips were constrained by developing or developed crystals. For the SC-90° in Fig. 7c, there were continuous supercooled melt between two

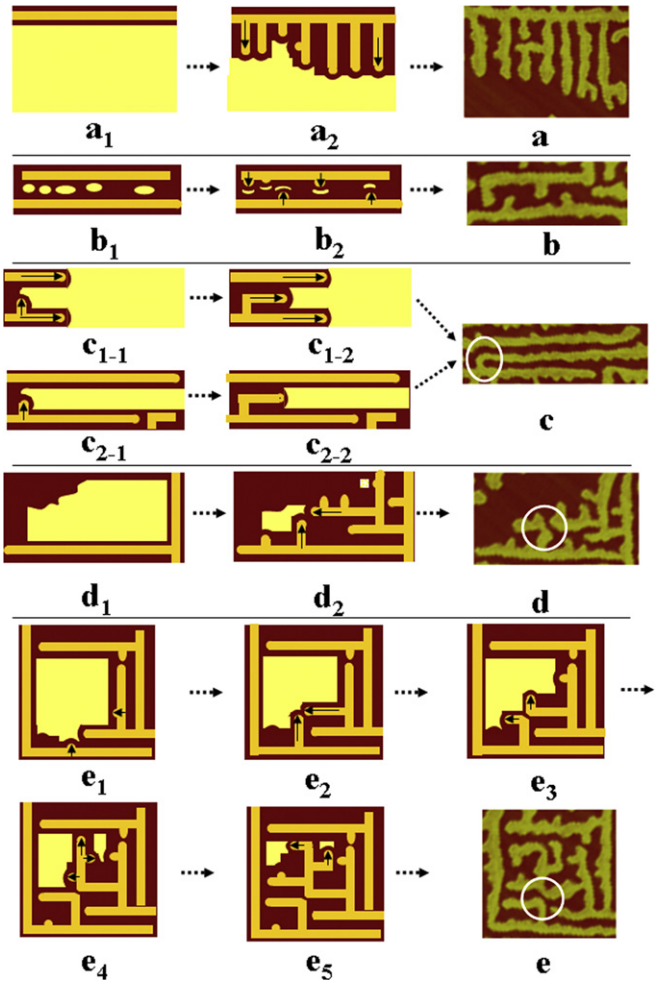

Fig. 7. Possible formation processes of different labyrinthine portions.

developing (as shown in Fig. 7c$_{1-1}$) or developed (as shown in Fig. 7c$_{2-1}$) crystal branches, and the distance between two developing or developed SCs is $d_{SC} \approx \bar{L} + 2\bar{d}_c$. The growth of the propagated crystal from the nether SC was constrained by the upper one, then it took a turn of 90° to keep growing as shown in Fig. 7c$_{1-2}$ and c$_{2-2}$. In the case of SC-90° in Fig. 7d, it is obvious that the distance between SC-90° and the neighbor tip is smaller than $2\bar{d}_c$. The possible formation process is as follows: Two growing crystals would collide as shown in Fig. 7d$_2$, and they should take turns to keep growing. However, the supercooled melt on the left were available for the nether one but not for the upper one. Then the nether one took a turn of 90° on the left to continuously grow, while the upper one stopped growing. Due to the confinements of two original SCs in Fig. 7d$_1$, the resultant portion is semi-closed. The formation of SC-90° signed in Fig. 7e seems much complex but actually similar to Fig. 7d. Two colliding crystals took turns at the same time because the supercooled melt were available for both of their tips as shown in Fig. 7e$_2$ and e$_3$. The formation process of the labyrinthine portion in Fig. 7e was much intricate because of the complex confinements of original developed SCs as shown in Fig. 7e$_1$. The growing crystals had to take several turns to keep growing as shown in Fig. 7e$_2$–e$_5$, then a quasi-closed portion finally formed in Fig. 7e.

3.6. Long period of labyrinthine patterns in width direction

Based on the FFT results, the value of $\bar{L}$can be calculated according to the expression $\bar{L} = y/Q_{peak}$, where y is the side length of AFM image. Fig. 8a presents the plots of $\bar{L}$ vs. T_c for different PEO fractions. $\bar{L}$ is composed of $2\bar{d}_c$ and $\bar{W}$, where both $\bar{d}_c$ and $\bar{W}$ are proportional to D_s/v,[11,76] so $\bar{L} \propto D_s/v$, where D_s is the diffusion coefficient of the molten macromolecules and v is the velocity of the growing crystal front. It is commonly accepted that D_s will increase but v will decrease with increasing T_c. So, the value of $\bar{L}$ for an individual PEO fraction gradually increases with increasing T_c as shown in Fig. 8a. Fig. 8b presents the plots of $\ln\bar{L}$ vs. $T_m^0/T_c\Delta T$ for different PEO fractions. The plots show a similar linear fitting with an average slope of 137.3 ± 15.5, which implies that $\bar{L}$ of different fractions exhibits a similar temperature dependence. We will discuss the temperature dependence in the following subsections.

3.7. Molecular weight dependence of labyrinthine pattern

The molecular weight dependence of physical properties is one of the most important characteristics in polymeric materials science. To better understand the local-diffusion-limited mechanism, we studied the molecular weight dependence of the labyrinthine patterns. Apparently, the highest T_c, at which labyrinthine pattern can form, increases with increasing molecular weight as shown in Fig. 8a. Fig. 9 clearly shows the long period $\bar{L}$ decrease with increasing molecular weight. Quantitatively, $\bar{L}$ obeys a power law of $\bar{L} \propto \bar{M}_w^{-0.24\pm0.03}$. This power law could be attributed to a molecular size dependence of $\bar{L} \propto R_{g||}^{-0.31\pm0.04}$, where $R_{g||}$ is the gyration radius of polymer chains parallel to the silicon surface in quasi-2D. In this study we assume $R_{g||} \propto \bar{M}_w^{0.75}$, a scaling relation had been widely accepted in 2D [25,77,78].

Constitutionally, the negative exponent value in the power law means that $\bar{L}$ decreases with increasing molecular weight or size. Then $\bar{d}_c$ also decreases with increasing molecular weight or size. This implies that the length increment of crystal growth forward is larger than the decrement of supercooled melt backward. This implication supports the local-diffusion-limited growth mechanism that is associated with the rapid crystal growth and relatively slow molecular diffusion. A crystal growth is composed of growths in the forward and transverse directions [14]. In this study we assume that the forward growth direction would be normal to (100) plane, and then the transverse growth direction is normal to (010) plane (in other words, growth face is (100) face). So, we could calculate the ideal macromolecule number, *MN*, to complete

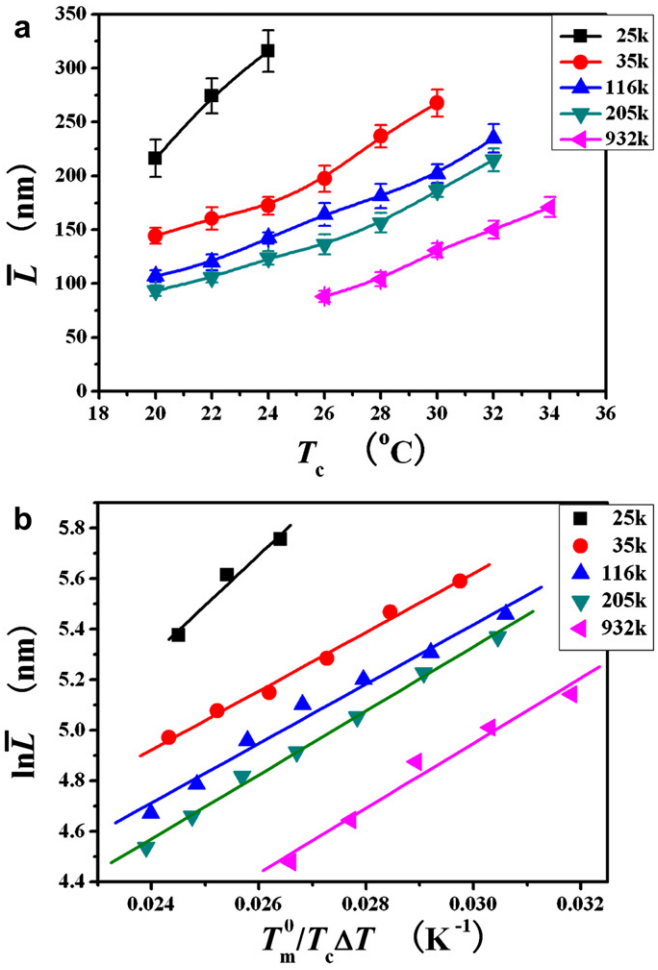

Fig. 8. (a) Plots of $\bar{L}$ vs. T_c of different PEO fractions. (b) Plots of $\ln\bar{L}$ vs. $T_m^0/T_c\Delta T$ of different PEO fractions. Linear fittings follow an average slope of 137.3 ± 15.5.

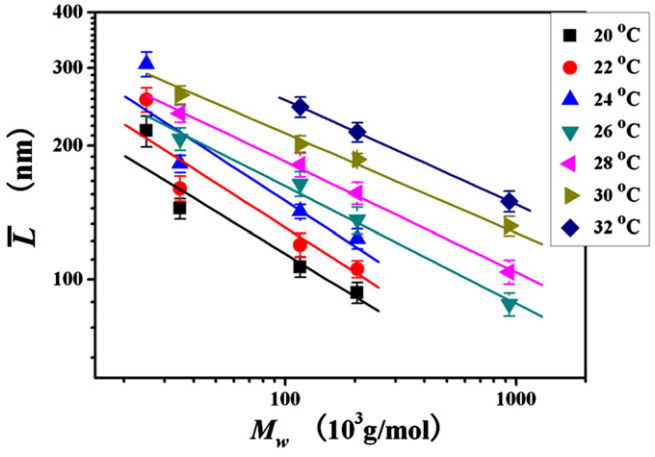

Fig. 9. *Log–log* plots of $\bar{L}$ vs. $\bar{M}_w$ at different T_c s. Linear fittings follow an average slope of −0.24 ± 0.03. The deviation of the data of 25k-PEO may be because its molecular weight is the onset of molecular weight for labyrinthine crystal pattern at $T_c \geq 20$ °C.

a transverse crystal layer for these PEO fractions as shown in Table 2. One can note that *MN* decreases with increasing molecular weight. For the fractions with $\overline{M}_w \geq 116,000$ g/mol, $MN < 1.0$ means that a macromolecule may join more than one SC crystal or, alternatively, incorporate into the same crystal to form more than one transverse layer. In the second case, a long macromolecule joining the same crystal will cause a much longer growth forward than a short macromolecule, which is indicative of the molecular weight dependence in the crystal growth process.

3.8. Theoretical molecular weight dependence of long period

In order to have a good understanding of the power law of $\overline{L} \propto \overline{M}_w^{-0.24\pm0.03}$, we should consider the complex molecular weight dependences of D_s and v in polymer crystallization processes. The complex kinetic-controlled crystallization contains following processes: (1) the molecular diffusion from the supercooled melt through depletion zone to crystal growing front; (2) the adsorption and incorporation of molecules onto growing front; (3) the relaxation of adsorbed molecules and diffusion of latent heat. In our experiments, the T_cs are so low that the molecules will immediately incorporate into crystal and latent heat will quickly diffuse away once the molecules adsorb onto growing front, and molecular relaxation can be ignored. Then molecular diffusion, denoted using D_s, and adsorption of molecular chains onto crystal growing front, A, are key steps controlling the crystallization process. Diffusion ability of polymer chains decreases with increasing molecular weight according to the power law of $D_s \propto \overline{M}_w^{-1.5}$ in quasi-2D [25,77]. To consider the molecular weight dependence of crystal growth velocity, v, can be expressed as: $v \propto AD_s \exp[-\Delta E/RT_c - K_g T_m^0/T_c \Delta T]$,[79–81] where ΔE is the activation energy for repetition in the melt and K_g is the nucleation constant. Here, ΔE is assumed to be independent of temperature because of our experimental relative narrow temperature range, and $\Delta E = 29.4$ kJ/mol [56] is used. ΔE and K_g show slight molecular weight dependence, so the molecular weight dependence of v can be simplified as $v \propto AD_s$. The molecular weight dependence of A can be expressed as $A \propto \overline{M}_w^{\beta}$, where β is a conformational parameter whose value is highly related to the conformation of adsorbed macromolecules [82]. In ultrathin films, polymer chains take a pancake-like conformation with $R_{g||} \propto \overline{M}_w^{0.75}$ in quasi-2D [25]. Since the "probing" mechanism of crystal growing front and "acceptance" mechanism are mostly based on van der Waals forces, which fade away beyond ~7 Å,[83] the pancake-like conformation of adsorbed macromolecules in the depletion zone would not change. In this case, the molecular weight dependence of adsorption is $A \propto \overline{M}_w / 2R_{g||} \propto \overline{M}_w^{0.25}$. Then the molecular weight dependence of v is $v \propto AD_s \propto \overline{M}_w^{-1.25}$. Consequently, we obtain a power law of $\overline{L} \propto D_s/v \propto \overline{M}_w^{-0.25}$. The theoretical value of −0.25 is in a good agreement with the experimental result of -0.24 ± 0.03. This further indicates that our assumption of $R_{g||} \propto \overline{M}_w^{0.75}$ is reasonable.

The scaling law consequentially results in different temperature dependences of the labyrinthine formation for different PEO fractions. At a specific T_c, for high-molecular-weight fractions ($\overline{M}_w > 25,000$), $\overline{L}$ may be smaller than a critical value, so the labyrinthine crystal patterns can be observed; for the lower molecular weight fractions ($\overline{M}_w < 25,000$), the value of $\overline{L}$ may exceed the critical value, then no labyrinthine but dendrite crystal patterns would form. Actually, the labyrinthine crystal pattern can only be observed for the PEO fractions with $\overline{M}_w \geq 25,000$ g/mol at $T_c \geq 20$ °C in our experiment. As to the PEO fractions with $\overline{M}_w < 25,000$, less entanglements between molecular chains and less adsorbing points of a chain onto silicon surface greatly strengthen the diffusion ability of macromolecules, and correspondingly the value of $\overline{L}$ is much large, thus the labyrinthine pattern formation may need a much lower T_c.

3.9. Temperature dependence of long period

Considering the temperature effects, $\overline{L}$ can be expressed as $\overline{L} \propto \overline{M}_w^{-0.24} \exp[\Delta E/RT_c + K_g T_m^0/T_c \Delta T]$. Then, the expression $\ln(\overline{L}/\overline{M}_w^{-0.24}) \propto \Delta E/RT_c + K_g T_m^0/T_c \Delta T$ can eliminate the molecular weight effect. According to the HL theory in polymer crystallization, $\Delta E/RT_c$ is the molecular transport term and $K_g T_m^0/T_c \Delta T$ is the secondary nucleation term. Fig. 10 shows the plots $\ln(\overline{L}/\overline{M}_w^{-0.24}) - \Delta E/RT_c$ vs. $T_m^0/T_c \Delta T$ of different PEO fractions. The values of these fractions can be fitted well using a linear master curve with a slope of 197.8 K except for the three points of 25k-PEO. The deviation of the data of 25k-PEO may be because its molecular weight is the onset of molecular weight for labyrinthine crystal pattern at $T_c \geq 20$ °C. The linear fitting indicates a secondary-nucleation-dominant temperature dependence of $\overline{L}$. The slope of the fitting line corresponds to the nucleation constant, K_g, in regime III. It is worth to mention that T_m^0 is not involved in K_g in our result. The value of $K_g = 197.8$ K is close the data recently reported for HMW PEO and LMW PEO both in bulk and in thin films [84–86].

3.10. Polymer chains joining crystal growing fronts

In three-dimensional (3D) space, random-coil polymer chains may fold forward and backward to form switchboard crystals [87]. In the switchboard model, stems of a polymer chain may join

Table 2
Ideal macromolecule number to complete a transverse crystal layer.

Sample designation	*M-FN*	$\overline{W}_{(nm)}$	*C-FN*	*MN*	$2R_{g\|\|}$, nm	$\overline{L}$, *nm*
25k-PEO	21	110.8	170	8.14	41.1	216.3
35k-PEO	30	75.9	116	3.90	52.9	144.3
116k-PEO	103	55.9	86	0.84	130.0	106.8
205k-PEO	184	48.6	75	0.41	199.3	93.4
932k-PEO	840	46.9	72	0.09	620.5	88.0

M-FN is the ideal folding number of an individual molecular chain calculated according to the equation $M - FN = (0.2783 \times \overline{M}_w)/(l_c \times 44) - 1$. $\overline{W}$ is the average width of SCs for 25k, 35k, 116k, 205k-PEO at 20 °C and 932k-PEO at 26 °C *C–FN* is the transverse folding number of an SC crystal, which is calculated based on the equation $C - FN = 2\overline{W}/b$, where $b = 1.304$ nm is the unit cell parameter in [010] direction. *MN* is the ideal macromolecule number to complete a transverse crystal layer, which is calculated according to the equation $MN = (C - FN + 1)/M - FN$.

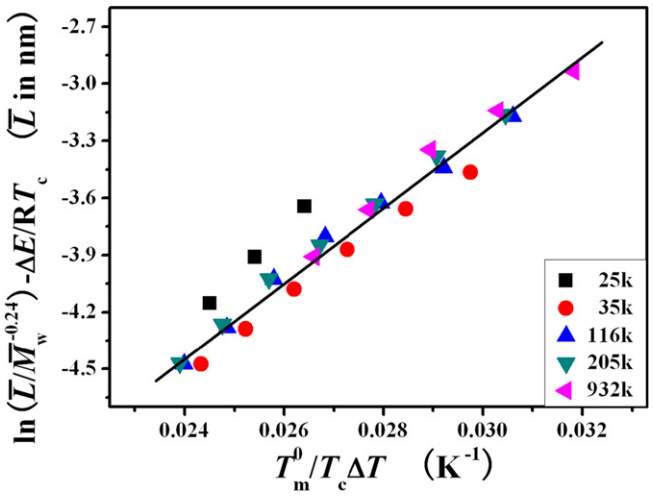

Fig. 10. Plot of $\ln(\overline{L}/\overline{M}_w^{-0.24}) - \Delta E/RT_c$ vs. $T_m^0/T_c\Delta T$ of different PEO fractions, and a linear master curve with a slope of 197.8 K except for the data of 25k-PEO.

different lamellae, and the interlayers contain chain segments of various lengths that connect the adjacent lamellae. In ultrathin films, polymer chains take a pancake-like conformation in quasi-2D space, and crystals on silicon surface are mono-layers. Then, the process of a polymer chain joining crystal growing front in ultrathin films may be different from that in 3D space. When $2R_{g||} < \bar{L}$, a polymer chain most likely joins an individual crystal branch. When $2R_{g||} > \bar{L}$, there are two possible cases: (1) A polymer chain joins an individual crystal branch; (2) A polymer chain joins different crystal branches. In the first case, some stems of a polymer chain form a secondary nucleus on a crystal growing front, and then other stems of the polymer chain follow the secondary nucleus to join the crystal branch. As shown in Fig. 11a, for example, the black chain and red chain join the crystal A_1 and B_1, respectively. In the second case, because our experiments were performed in Regime III, multiple secondary nuclei made it possible that stems in one polymer chain might nucleate on different crystal growing fronts, then the polymer chain may join more than one crystal branch. Actually, in this case, the HL theory may be consistent with the precursor theory to some extent. A pancake-like polymer can be divided into many "blobs" (or quasi-2D discs) derived from blob theory [88]. According to the precursor theory, mesomorphic layers firstly form and then transform to be granular crystalline layers within a "blob". At last, the granular crystalline layers within a blob join a crystal branch. Statistically, the motion of every blob should be independent, and they may join different crystal branches. As Fig. 11b shown, the black blob and red blob join the crystal A_2 and B_2, respectively. The neighbor crystal branches are connected by uncrystallizing loops in the second case.

At low crystallization temperatures, the HL theory and precursor theory seem to have a similar meaning because the barrier of either secondary nucleation or forming granular crystalline layer is low and similar. Then, in our experimental conditions, a polymer chain is most likely to join different crystal branches as the second case. At high crystallization temperatures, the barrier of forming granular crystalline layers is too high, so the HL theory seems more reasonable than the precursor theory. Because of single or pauci secondary nuclei in a polymer chain, a polymer chain joining crystal should take the first case. Once a secondary nucleus forms on the growing front, other stems of the polymer chain may join the same crystal branch following the secondary nucleus as demonstrated in Fig. 11a.

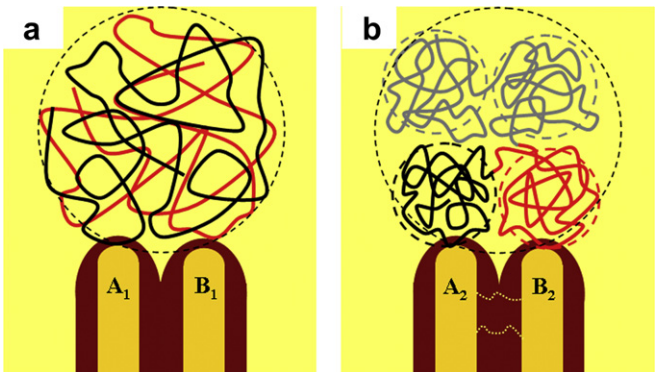

Fig. 11. Possible processes of a polymer chain joining growing fronts when $2R_{g||} > \bar{L}$. (a) A polymer chain joining an individual crystal branch. The black chain joining the crystal A_1. The red chain joining the crystal B_1. (b) A polymer chain joining different crystal branches based on blob theory. The polymer is composed of more than one blob. The black blob joins the crystal A_2. The red blob joins the crystal B_2. The dot lines between two branches represent uncrystallizing loops which connect neighbor branches. (For interpretation of the references to colour in this figure legend, the reader is referred to the web version of this article.)

4. Conclusion

In conclusion, a local-diffusion field condition was realized in supercooled molten ultrathin films of HMW PEO fractions at the condition far from equilibrium. This crystallization condition leads to the formation of labyrinthine crystal patterns with a periodic feature. The slow molecular diffusion and rapid crystal growth implied a local-diffusion-limited growth mechanism different from the conventional DLA model. The scaling relation between the long period in the crystal width direction and molecular weight $\bar{L} \propto \overline{M}_w^{-0.24\pm0.03}$ strongly supported our conclusion that the local-diffusion-limited growth mechanism resulted in the labyrinthine patterns. This mechanism can provide a basic understanding of the liquid/melt-to-solid phase transition behaviors in similar conditions. According to the HL theory, secondary nucleation dominated the temperature dependence of $\bar{L}$. The HL theory and precursor theory had a similar meaning in our experiments, which implied a polymer chain might join different crystal branches when $2R_{g||} > \bar{L}$.

Acknowledgments

Nankai group greatly appreciates National Science Foundation of China for a grant (NSFC20474033 and 20874053) to support this work. A.-C. Shi acknowledges the support from the Natural Science and Engineering Research Council of Canada.

References

[1] Ball P. The self-made tapestry: pattern formation in nature. Oxford University Press; 2001.
[2] Mullins WW, Sekerka RF. J Appl Phys 1964;35:444.
[3] Langer JS. Rev Mod Phys 1980;52:1.
[4] Meakin P. Fractals, scaling and growth far from equilibrium. Cambridge: Cambridge University Press; 1997.
[5] Lovinger AJ, Cais RE. Macromolecules 1984;17:1939.
[6] Phys Vicsek T. Rev Lett 1984;53:2281.
[7] Fowler AD, Stanley HE, Daccord G. Nature (London) 1989;341:134.
[8] Hwang RQ, Schröder J, Günther C, Behm R. Phys Rev Lett 1991;67:3279.
[9] Lereah Y, Zarudi I, Crünbaum E, Deutscher G. Phys Rev E 1994;49:649.
[10] Utter B, Ragnarsson R, Bodenschatz E. Phys Rev Lett 2001;86:4604.
[11] Reiter G, Sommer JU. Phys Rev Lett 1998;80:3771;
J Chem Phys 2000;112:4376.
[12] Taguchi K, Miyaji H, Izumi K, Hoshino A, Miyamoto Y, Kokawa R. Polymer 2001;42:7443.
[13] Zhai X, Wang W, Zhang G, He B. Macromolecules 2006;39:324.
[14] Zhang G, Jin L, Ma Z, Zhai X, Yang M, Zheng P, et al. Chem Phys 2008;129:224708.
[15] Jin L, Zhang G, Zhai X, Ma Z, Zheng P, Wang W. Polymer 2009;50:6157.
[16] Witten TA, Sander LM. Phys Rev Lett 1981;47:1400;
Phys Rev B 1983;27:5686.
[17] Barabási A-L, Stanley HE. Fractal concepts in surface growth. Cambridge: Cambridge University Press; 1995.
[18] Brener EA, Temkin DE. Europhys Lett 1989;10:171.
[19] Galenko PK, Krivilyov MD. Modelling Simul Mater Sci Eng 2000;8:81.
[20] Shibkov AA, Zheltov MA, Korolev AA, Kazakov AA, Leonov AA. J. Crystal Growth 2005;285:215.
[21] Chaikin PM, Lubensky TC. Principles of condensed matter physics. New York: Cambridge University Press; 1995.
[22] Cheng SZD. Phase transitions in polymers: the role of metastable states. Elsevier Science; 2008.
[23] Ma Z, Zhang G, Zhai X, Jin L, Tang X, Zheng P, et al. Polymer 2008;49:1629.
[24] Jones RAL. Curr. Opin. Colloid Interface Sci 1999;4:153.
[25] Sukhishvili SA, Chen Y, Müller JD, Gratton E, Schweizer KS, Granick S. Nature (London) 2000;406:146.
[26] Fryer DS, Peters RD, Kim EJ, Tomaszewski JE, Pablo JJ, Nealey PF, et al. Macromolecules 2001;34:5627.
[27] Schönherr H, Frank CW. Macromolecules 2003;36:1188.
[28] Wunderlich B. Macromolecular physics, vols. 1 and 2. New York: Academic; 1976.
[29] Armistead K, Goldbeck-Wood G. Adv Polym Sci 1992;100:219.
[30] Keller A, Cheng SZD. Polymer 1998;39:4461.
[31] Lauritzen JIJ, Hoffman JD. J Res Nat Bur Std 1960;64A:37.
[32] Strobl G. Eur Phys J E 2000;3:165.
[33] Kovacs AJ, Gonthier A, Kolloid- ZuZ. Polymere 1972;250:530.
[34] Kovacs A, Gonthier A, Straupe C. J Polym Sci Polym Symp 1975;50:283.
[35] Kovacs A, Straupe C, Gonthier A. J Polym Sci Polym Symp 1977;59:31.

[36] Kovacs A, Straupe C. Faraday Discuss Chem Soc 1979;68:225.
[37] Kovacs A, Straupe CJ. Cryst Growth 1980;48:210.
[38] Shimadab T, Okui N, Kawai T. Makromol Chem 1980;181:2643.
[39] Cheng SZD, Wunderlich B. Macromolecules 1989;22:1866.
[40] Cheng SZD, Zhang A, Chen J. J Polym Sci Part C Polym Lett 1990;28:233.
[41] Cheng SZD, Zhang A, Chen J, Heberer DP. J Polym Sci Part B Polym Phys 1991;29:287.
[42] Cheng SZD, Chen J, Zhang A, Heberer DP. J Polym Sci Part B Polym Phys 1991;29:299.
[43] Cheng SZD, Chen J, Zhang A, Barley JS. Polymer 1992;33:1140.
[44] Cheng SZD, Chen J, Barley JS, Zhang A. Macromolecules 1992;25:1453.
[45] Cheng SZD, Wu SS, Chen J, Zhou Q, Quirk R. Macromolecules 1993;26:5105.
[46] Lee S-W, Chen E, Zhang A, Yoon Y, Moon BS, Lee S, et al. Macromolecules 1996;29:8816.
[47] Chen E-Q, Lee S-W, Zhang A, Moon BS, Mann I, Harris FW, et al. Macromolecules 1999;32:4784.
[48] Zhai XM, Wang W, Ma ZP, Wen XJ, Yuan F, Tang XF, et al. Macromolecules 2005;38:1717.
[49] Tang XF, Wen XJ, Zhai XM, Xian N, Wang W, Wegner GJ, et al. Macromolecules 2007;40:4386.
[50] Delaite E, Point JJ, Dammam P, Dosière M. Macromolecules 1992;25:4768.
[51] Point JJ, Damman P, Janimak JJ. Polymer 1993;34:3771.
[52] Point JJ. Macromolecules 1997;30:1375.
[53] Chen E-Q, Jing AJ, Weng X, Huang P, Lee S-W, Cheng SZD, et al. Polymer 2003;44:6051.
[54] Zhu D-S, Liu Y-X, Chen E-Q, Li M, Chen C, Sun Y-H, et al. Macromolecules 2007;40:1570.
[55] Liu Y-X, Li J-F, Zhu D-S, Chen E-Q, Zhang H- D. Macromolecules 2009;42:2886.
[56] Cheng SZD, Chen J, Janimak JJ. Polymer 1990;31:1018.
[57] Marentette JM, Brown GR. Polymer 1998;39:1405.
[58] Schultz JM, Miles MJ. J Polym Sci Part B Polym Phys 1998;36:2311.
[59] Schönherr H, Frank CW. Macromolecules 2003;36:1199.
[60] Ries ME, Brereton MG, Cruickshank JM, Klein PG, Ward IM. Macromolecules 1995;28:3282.
[61] Rosensweig RE, Zahn M, Shumovich RJ. Magn Magn Mater 1983;39:127.
[62] Petrich DM, Goldstein RE. Phys Rev Lett 1994;72:1120.
[63] Petrov V, Ouyang Q, Swinney HL. Nature (London) 1997;388:655.
[64] Collet P. Int J Bifurcat Chaos 2002;12:2445.
[65] Rougeaille N, Gabaly FE, Stumpf R, Schmid AK, Thürmer K, Bartelt NC, et al. Phys Rev Lett 2007;99:106101.
[66] Sandnes B, Knudsen HA, Måløy KJ, Flekkøy EG. Phys Rev Lett 2007;99:038001.
[67] Lotz B, Kovacs AJ. Kolloid ZZ Polym 1966;209:97.
[68] Takahashi Y, Tadakoro H. Macromolecules 1973;6:672.
[69] Meyer E, Braun H- G. J Phys: Condensed Matter 2005;17:S623.
[70] Braun H-G, Meyer E. J Phys Conf Ser 2008;126:012027.
[71] Simon FT, Rutherford JM. J Appl Phys 1964;35:82.
[72] Bi W, Teguh JS, Yeow EKL. Phys Rev Lett 2009;102:048302.
[73] Keddie JL, Jones RAL, Cory RA. Faraday Discuss 1994;98:219; Europhys Lett 1994;27:59.
[74] Torres JA, Nealey PF, de Pablo JJ. Phys Rev Lett 2000;85:3221.
[75] Fryer DS, Peters RD, Kim EJ, Tomaszewski JE, de Pablo JJ, Nealey PF. Macromolecules 2001;34:5627.
[76] Keith HD, Padden FJ. J Appl Phys 1963;34:2409.
[77] Sukhishvili SA, Chen Y, Müller JD, Gratton E, Schweizer KS, Granick S. Macromolecules 2002;35:1776.
[78] Desai TG, Keblinski P, Kumar SK, Granick S. Phys Rev Lett 2007;98:218301.
[79] Umemoto S, Okui N. Polymer 2005;46:8790.
[80] Okui N, Umemoto S. Polymer crystallization. In: Sommer JU, Reiter G, editors. Observations, concepts and interpretations. Berlin: Springer; 2003. p. 343.
[81] Okui N, Umemoto S, Kawano R, Mamun A. In: Reiter G, Strobl G, editors. Progress in understanding of polymer crystallization. Berlin: Springer; 2007. p. 391.
[82] Sato T, Richard R. Stabilization of colloidal dispersions by polymer adsorption. In: Surface science series 9. New York: Marcel Dekker; 1980.
[83] Lotz B. Eur Phys J E 2000;3:185.
[84] Huang XD, Goh SH. Macromolecules 2001;34:3302.
[85] Kuo S-W, Huang W-J, Huang C-F, Chan S-C, Chang F-C. Macromolecules 2004;37:4164.
[86] Shafee EE. Polym Int 2004;53:249.
[87] Flory PJ. J Am Chem Soc 1962;84:2857.
[88] Brochard F, de gennes PG. J Chem Phys 1977;67:52.